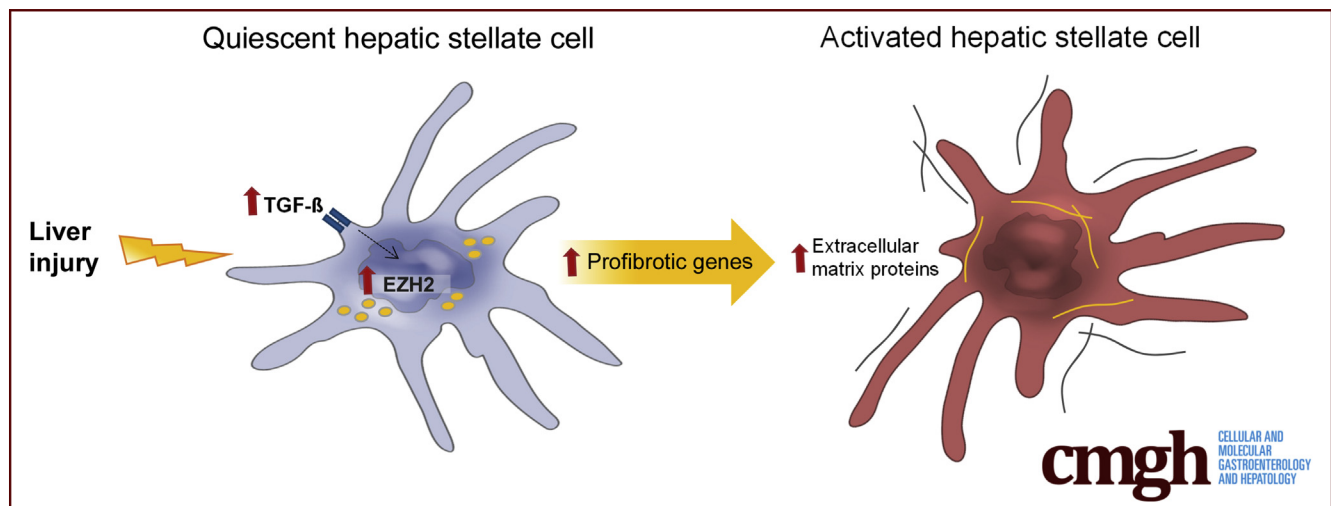


ORIGINAL RESEARCH

Enhancer of Zeste Homologue 2 Inhibition Attenuates
TGF- β Dependent Hepatic Stellate Cell Activation and
Liver Fibrosis

Rosa Martin-Mateos,^{1,2} Thiago M. De Assuncao,¹ Juan Pablo Arab,^{1,3} Nidhi Jalan-Sakrikar,¹ Usman Yaqoob,¹ Thomas Greuter,¹ Vikas K. Verma,¹ Angela J. Mathison,^{4,5} Sheng Cao,¹ Gwen Lomber,⁵ Philippe Mathurin,⁶ Raul Urrutia,^{4,5} Robert C. Huebert,¹ and Vijay H. Shah¹

¹Division of Gastroenterology and Hepatology, Mayo Clinic, Rochester, Minnesota; ²Division of Gastroenterology and Hepatology, Ramón y Cajal University Hospital, Madrid, Spain; ³Departamento de Gastroenterología, Escuela de Medicina, Pontificia Universidad Católica de Chile, Santiago, Chile; ⁴Genomics and Precision Medicine Center (GSPMC), Medical College of Wisconsin, Milwaukee, Wisconsin; ⁵Division of Research, Department of Surgery, Medical College of Wisconsin, Milwaukee, Wisconsin; and ⁶Service Maladie de l'Appareil Digestif, INSERM U995 Université Lille 2, Centre Hospitalier Régionale Universitaire (CHRU) de Lille, France



SUMMARY

The histone methyltransferase enhancer of zeste homologue 2 promotes transforming growth factor- β -dependent hepatic stellate cell activation. Consistent with this function, enhancer of zeste homologue 2 inhibition attenuates stellate cell activation and fibrosis induced by carbon tetrachloride or bile duct ligation.

BACKGROUND & AIMS: Transdifferentiation of hepatic stellate cells (HSCs) into myofibroblasts is a key event in the pathogenesis of liver fibrosis. Transforming growth factor β (TGF- β) and platelet-derived growth factor (PDGF) are canonical HSC activators after liver injury. The aim of this study was to analyze the epigenetic modulators that differentially control TGF- β and PDGF signaling pathways.

METHODS: We performed a transcriptomic comparison of HSCs treated with TGF- β or PDGF-BB using RNA sequencing. Among the targets that distinguish these 2 pathways, we

focused on the histone methyltransferase class of epigenetic modulators.

RESULTS: Enhancer of zeste homolog 2 (EZH2) was expressed differentially, showing significant up-regulation in HSCs activated with TGF- β but not with PDGF-BB. Indeed, EZH2 inhibition using either a pharmacologic (GSK-503) or a genetic (small interfering RNA) approach caused a significant attenuation of TGF- β -induced fibronectin, collagen 1 α 1, and α -smooth muscle actin, both at messenger RNA and protein levels. Conversely, adenoviral overexpression of EZH2 in HSCs resulted in a significant stimulation of fibronectin protein and messenger RNA levels in TGF- β -treated cells. Finally, we conducted in vivo experiments with mice chronically treated with carbon tetrachloride or bile duct ligation. Administration of GSK-503 to mice receiving either carbon tetrachloride or bile duct ligation led to attenuated fibrosis as assessed by Trichrome and Sirius red stains, hydroxyproline, and α -smooth muscle actin/collagen protein assays.

CONCLUSIONS: TGF- β and PDGF share redundant and distinct transcriptomic targets, with the former predominating in HSC activation. The EZH2 histone methyltransferase

is preferentially involved in the TGF- β as opposed to the PDGF signaling pathway. Inhibition of EZH2 attenuates fibrogenic gene transcription in TGF- β -treated HSCs and reduces liver fibrosis in vivo. The data discussed in this publication have been deposited in NCBI's Gene Expression Omnibus and are accessible through GEO Series accession number GSE119606 (<https://www.ncbi.nlm.nih.gov/geo/query/acc.cgi?acc=GSE119606>) (*Cell Mol Gastroenterol Hepatol* 2019;7:197-209; <https://doi.org/10.1016/j.jcmgh.2018.09.005>)

Keywords: EZH2; Liver Fibrosis; Epigenetics; Histone Modifications.

See editorial on page 237.

Cirrhosis, as the last stage of chronic liver diseases, is characterized by the accumulation of extracellular matrix (ECM), chronic inflammation, and fibrosis.¹ Hepatic stellate cells (HSCs) constitute the primary source of ECM once they transdifferentiate into myofibroblasts.² Transforming growth factor β (TGF- β) and platelet-derived growth factor (PDGF) are key growth factor ligands that drive the transdifferentiation process.³ TGF- β binding to the type I receptor induces phosphorylation of downstream SMAD proteins, which ultimately promotes transcription of matrix components.⁴ PDGF, on the other hand, is one of the best-known mitogens for HSCs.⁵ A better understanding of the redundant and distinct pathways that control TGF- β and PDGF-dependent HSC activation may lead to more refined approaches for potential therapeutic benefit.

Epigenetics defines the reversible and inheritable changes in gene expression that do not alter the underlying DNA sequence.⁶ Epigenetic modifications act coordinately to configure cell type and context-specific gene transcription programs. DNA methylation, noncoding RNAs, and histone modifications encompass mechanisms of epigenetic regulations. With regard to the latter, histone modifications such as methylation, acetylation, ubiquitination, or phosphorylation lead to reversible changes in chromatin structure and consequently to transcriptional gene activation or repression.⁷ Enhancer of zeste homologue 2 (EZH2) is a histone methyltransferase responsible for the trimethylation of histone 3 at lysine 27 (H3K27me3). This epigenetic mark promotes chromatin compaction and silencing of gene transcription.⁸ EZH2 mediates transcriptional repression of several tumor-suppressor genes,^{9,10} promoting proliferation and metastasis. Some evidence also suggests that EZH2 may promote fibrosis,¹¹⁻¹³ but its specific role in the TGF- β signaling pathway during HSC transdifferentiation has not been addressed.

In this study, we first sought to characterize the epigenetic mechanisms involved in TGF- β - vs PDGF-specific signaling pathways during HSC activation. For an unbiased approach, we first performed RNA sequencing to compare gene expression profiles in primary human HSCs treated with either TGF- β or PDGF. We found that among histone methyltransferases (HMTs), EZH2 expression increased in HSCs treated with TGF- β but not with PDGF,


which led us to hypothesize that EZH2 is specifically involved in TGF- β dependent profibrotic pathways. To further explore the role of EZH2 in fibrogenesis, we tested the effect of either genetic (small interfering RNA [siRNA]) or pharmacologic (GSK-503) EZH2 inhibition. Our results show that EZH2 inhibition attenuates fibrogenic gene transcription and protein expression in TGF- β -activated HSCs. Conversely, EZH2 adenoviral overexpression promoted production of matrix proteins. In vivo, we found that EZH2 inhibition attenuates liver fibrosis in the carbon tetrachloride (CCL₄) and bile duct ligation (BDL) murine models. This work provides further understanding of the complex network of epigenetic changes that occur during liver fibrogenesis and shows the profibrotic role of EZH2 in HSCs in vitro and in vivo. Our findings suggest that targeting epigenetic modulators involved in HSC activation such as EZH2 could be useful for future liver fibrosis therapies.

Results

TGF- β Shares Overlapping Targets With PDGF but Has a More Dominant Role in HSC Activation

To compare TGF- β and PDGF signaling pathways using an unbiased approach, we performed RNA sequencing in primary human HSCs treated with TGF- β or PDGF-BB for 2 hours after overnight serum starvation. A whole-genome expression heat map comparing basal vs TGF- β and PDGF-BB stimulation gene expression showed that these dominant HSC regulatory growth factors overlap in terms of the activation and repression of multiple targets (Figure 1A). The analysis of the top 10 activated canonical pathways using Ingenuity Pathway Analysis (IPA, Qiagen Inc, Hilden, Germany) software also showed substantial overlapping roles (Figure 1B). A Venn diagram confirmed that both concur on the significant regulation of 112 specific genes (Table 1) implicated in a wide range of biological activities (gene selection criteria: log fold change >1.5 and false discovery rate [FDR] < 0.05) (Figure 1C). However, the hepatic fibrosis/HSC activation pathway was highly significant for the TGF- β data set (-log[P value], 5.6), whereas treatment with PDGF-BB was not as dominant as TGF- β for this domain (-log[P value], 2.686) (Figure 1D). Interestingly, HSC stimulation with both TGF- β and PDGF-BB showed increased cell migration activity

Abbreviations used in this paper: BDL, bile duct ligation; CCL₄, carbon tetrachloride; CHIP, chromatin immunoprecipitation; CTGF, connective tissue growth factor; DKK1, Dickkopf-1; ECM, extracellular matrix; EZH2, enhancer of zeste homologue 2; FBS, fetal bovine serum; FDR, false discovery rate; H3K27me3, trimethylation of histone 3 at lysine 27; HCC, hepatocellular carcinoma; HMT, histone methyltransferase; HSC, hepatic stellate cell; IP, intraperitoneally; IPA, Ingenuity Pathway Analysis; logFC, logarithmic fold change; mRNA, messenger RNA; PCR, polymerase chain reaction; PDGF, platelet-derived growth factor; siRNA, small interfering RNA; α -SMA, α -smooth muscle actin; TGF- β , transforming growth factor β ; VEGFA, vascular endothelial growth factor A; WT, wild type.

 Most current article

© 2019 The Authors. Published by Elsevier Inc. on behalf of the AGA Institute. This is an open access article under the CC BY license (<https://creativecommons.org/licenses/by/4.0/>).

2352-345X

<https://doi.org/10.1016/j.jcmgh.2018.09.005>

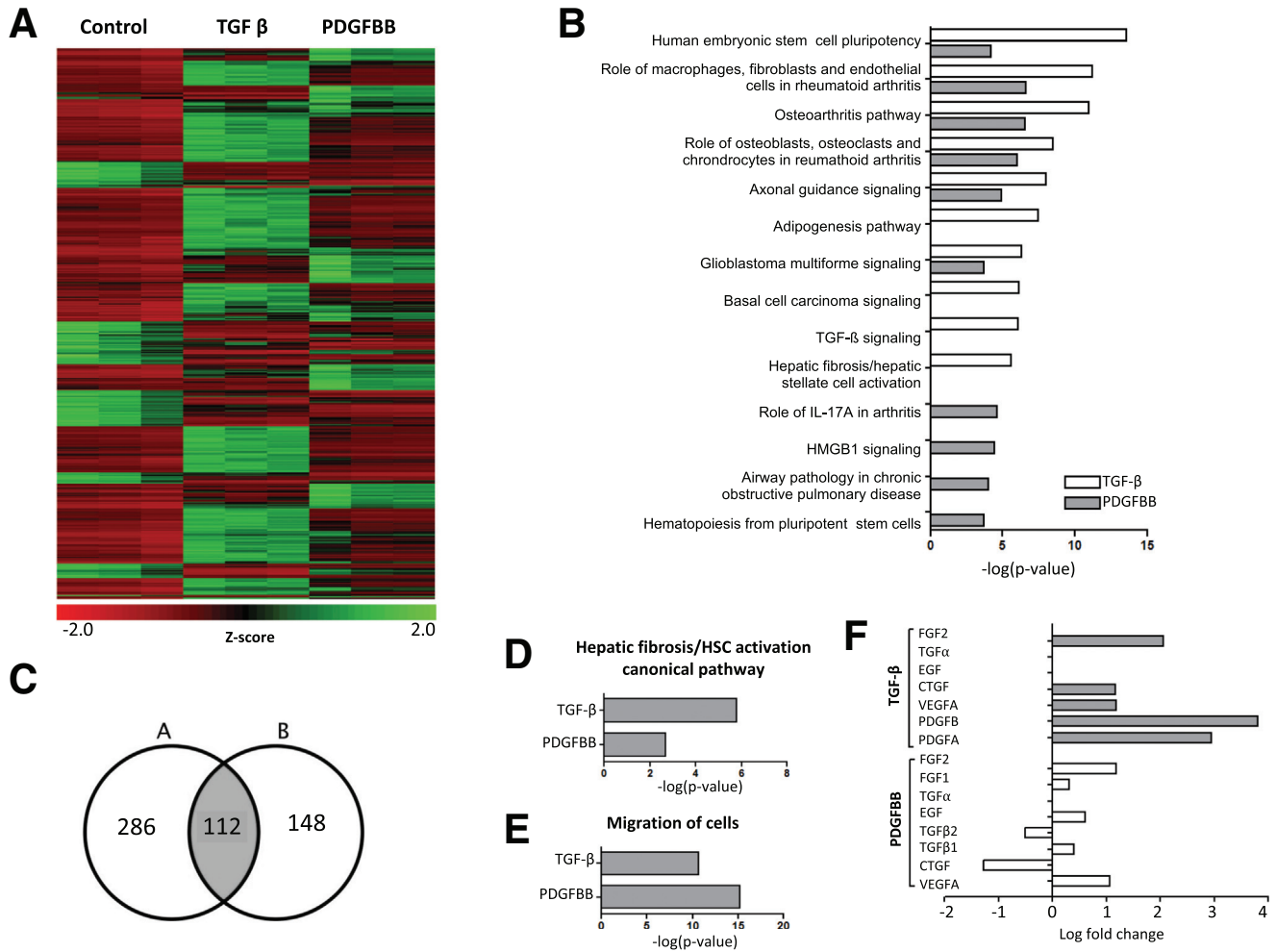


Figure 1. TGF- β shares overlapping targets with PDGF but has a predominant role in early HSC activation. Primary human HSCs were treated with either TGF- β or PDGF-BB for 2 hours. RNA sequencing was performed. (A) Whole-genome expression heat map presenting basal gene expression and changes after TGF- β and PDGF-BB stimulation showed overlapping regulation of multiple genes. (B) IPA showed overlapping roles regarding the top 10 canonical pathways activated after TGF- β and PDGF-BB treatment. (C) By using FDR of 0.05 and $\log_{2}FC > 1.5$ as selection criteria, a Venn diagram showed that TGF- β and PDGF concurred in the regulation of 112 different genes implicated in a wide range of biological functions. (D) Hepatic fibrosis and the HSC activation pathway was more relevant for the TGF- β data set (5.8 $-\log[P]$ value). (E) Cell migration activity was increased significantly either with TGF- β ($-\log[P]$ value, 10.670) or PDGF-BB (15.185 $-\log[P]$ value). (F) Comparison analysis of different growth factors showed that TGF- β stimulation induces up-regulation of PDGFA (logFC, 2.949), PDGFB (logFC, 3.806), VEGFA (logFC, 1.1836), CTGF (logFC, 1.163), and fibroblast growth factor 2 (FGF2) (logFC, 2.0640). Results from 3 independent experiments each performed in triplicate are shown. EGF, epidermal growth factor; IL, interleukin.

(TGF- β $-\log[P]$ value, 10.670; and PDGF-BB $-\log[P]$ value, 15.185) (Figure 1E). In addition, TGF- β treatment led to a significant increase in other fibrogenic growth factors such as PDGFA (2.949 logarithmic fold change [logFC]), PDGFB (3.806 logFC), vascular endothelial growth factor (VEGFA) (1.1836 logFC), connective tissue growth factor (CTGF) (1.163 logFC), or fibroblast growth factor 2 (2.0640 logFC). On the other hand, PDGF had little effect on TGF- β (TGF- β 1, 0.398 logFC; TGF- β 2, -0.503 logFC) or VEGFA expression (1.061 logFC), and also led to a decrease in CTGF (-1.271 logFC) (Figure 1F). All of these observations support the key role of TGF- β in HSC activation, which may predominate over PDGF effects despite sharing multiple target genes based on RNA sequencing.

EZH2 Is Up-Regulated in HSCs Treated With TGF- β but Not With PDGF-BB

Given our interest in epigenetic mediators and, specifically, histone modifications, we examined differences in this domain. We found that, in particular, HMT EZH2 was expressed differentially after TGF- β and PDGF-BB treatment, with a significant increase in expression after treatment with TGF- β (fold change, 1.52; $P = 8.25E-11$; FDR, 6.95E-10), but not with PDGF (fold change, -0.77, $P = 2.76E-04$; FDR, 9.90E-4) (Figure 2A). By using the following as selection criteria: log fold change, ≥ 1.5 ; $P < .05$, and FDR < 0.05 , IPA identified EZH2 as an upstream regulator (activation z-score, 1.444) (Figure 2B), which

Table 1. Alphabetical List of Genes Regulated by Both TGF- β and PDGF-BB

ADM	DKK1	HES4	NFATC2	RAP1GAP2
AMOTL2	E2F7	HEYL	NIPAL4	RASD1
ANGPTL4	EFR3B	HOXB-AS2	NKX3-1	RHBDL3
ANKRD33B	EGR3	IFIT2	NPTX1	RHOB
ARAP2	ELFN1	IFNE	NR4A1	RPL39P5
AXIN2	ENC1	IL6	NR4A3	RRAD
BBC3	EPHB3	IL11	OLFM2	RUNX1T1
BMF	ESM1	INHBA	PCDH1	SCG2
BMP2	FAM131B	KCNG1	PDGFA	SEMA7A
BMP4	FAM196A	KCNN4	PDGFB	SPDL1
C3orf52	FAM196B	KIAA1644	PGBD5	SPHK1
C8orf4	FBXO32	KIT	PITPNM3	SPRY2
CACNA1G	FGF18	KREMEN2	PKP1	STC1
CARMIL2	FGFR3	LIF	PLAUR	TAGLN3
CCNG2	FOSB	LOC401472	PLCH2	TCF7
CEBPD	GAL	LOC541472	PLEKHF1	TFPI2
CECR6	GAS1	LOC105376292	PNP	TNFAIP8L3
CLDN4	GCSAM	LRR8C	PNRC1	TRAF1
CNKSR3	GEM	LURAP1L	PODXL	WNT7B
CREBRF	GFPT2	MGC20647	PTCH1	ZNF365
CTTNBP2	GPR3	MIR17HG	PTGS2	
CXCL8	GREM2	MMP1	PTHLH	
DDIT4	HBEGF	NFATC1	PTPRE	

NOTE. LogFC > 1.5 and FDR < 0.05.
FGF, fibroblast growth factor.

supports that EZH2 is a mediator in TGF- β -driven HSC activation. These findings were replicated at the messenger RNA (mRNA) level (Figure 2C). Next, to evaluate temporal kinetics of TGF- β induction of EZH2 and its other transcriptional targets, we repeated RNA sequencing of primary human HSCs treated with TGF- β for 48 hours. Comparison analysis between the TGF- β effect at 2 vs 48 hours in HSCs showed greater activation of the hepatic fibrosis/HSC activation pathway (Figure 2D), which correlated with up-regulation of key myofibroblastic and fibrogenic genes such as α -smooth muscle actin (α -SMA) (logFC, 2.785; $P = 1.25E-161$), fibronectin 1 (logFC, 2.860; $P = 5.95E-111$), or collagen 1 α 1 (logFC, 1.002; $P = 2,04E-19$) at 48 hours (Figure 2E). The results also showed a sustained up-regulation of EZH2 at this time point as well (fold change, 1.6; $P = 3.89E-09$; FDR, 7.86E-08) (Figure 2F). The changes in EZH2 expression with TGF- β and PDGF at 48 hours were confirmed at the mRNA and protein levels (Figure 2G-I). Finally, to translate these findings into a clinical context, we analyzed liver tissue from healthy controls ($n = 5$) and explants from patients with alcoholic hepatitis undergoing early liver transplantation ($n = 7$).¹⁴ mRNA sequencing and chromatin immunoprecipitation (ChIP) sequencing for H3K27me3 was performed and the epigenetic and transcriptional profiles were analyzed. The RNA sequencing analysis using IPA identified EZH2 as a highly significant upstream

regulator in patients with alcoholic hepatitis (activation z-score, 2.453; P value of overlap = 3.92 E-10). Up-regulated genes consistent with activation of EZH2 are shown in Figure 2J. ChIP sequencing confirmed a gain in H3K27me3 at the promoter region of peroxisome proliferator-activated receptor γ and Dickkopf-1 (DKK1) in patients with alcoholic hepatitis as compared with healthy controls. These genes have been described previously as negative regulators of liver fibrosis (Figure 2K). Together, these data highlight important distinctions of TGF- β and PDGF RNA epigenetic targets including TGF- β selectivity for induction of EZH2 expression and its role in liver fibrosis.

EZH2 Inhibition Attenuates TGF- β -Dependent HSC Activation In Vitro

We next sought to examine whether EZH2 inhibition, either with pharmacologic or genetic approaches, would modulate HSC activation in vitro. First, we used an epigenetic compound, GSK-503, which specifically targets the catalytic subunit of EZH2.^{15,16} Inhibition of EZH2 in cells treated with GSK-503 and TGF- β led to a significant decrease in fibronectin, α -SMA, and collagen 1 α 1, both at mRNA and protein levels (Figure 3A and B). Parallel to this effect, we confirmed a significant down-regulation of H3K27me3 measured by Western blot and immunofluorescence (Figure 3C and D).

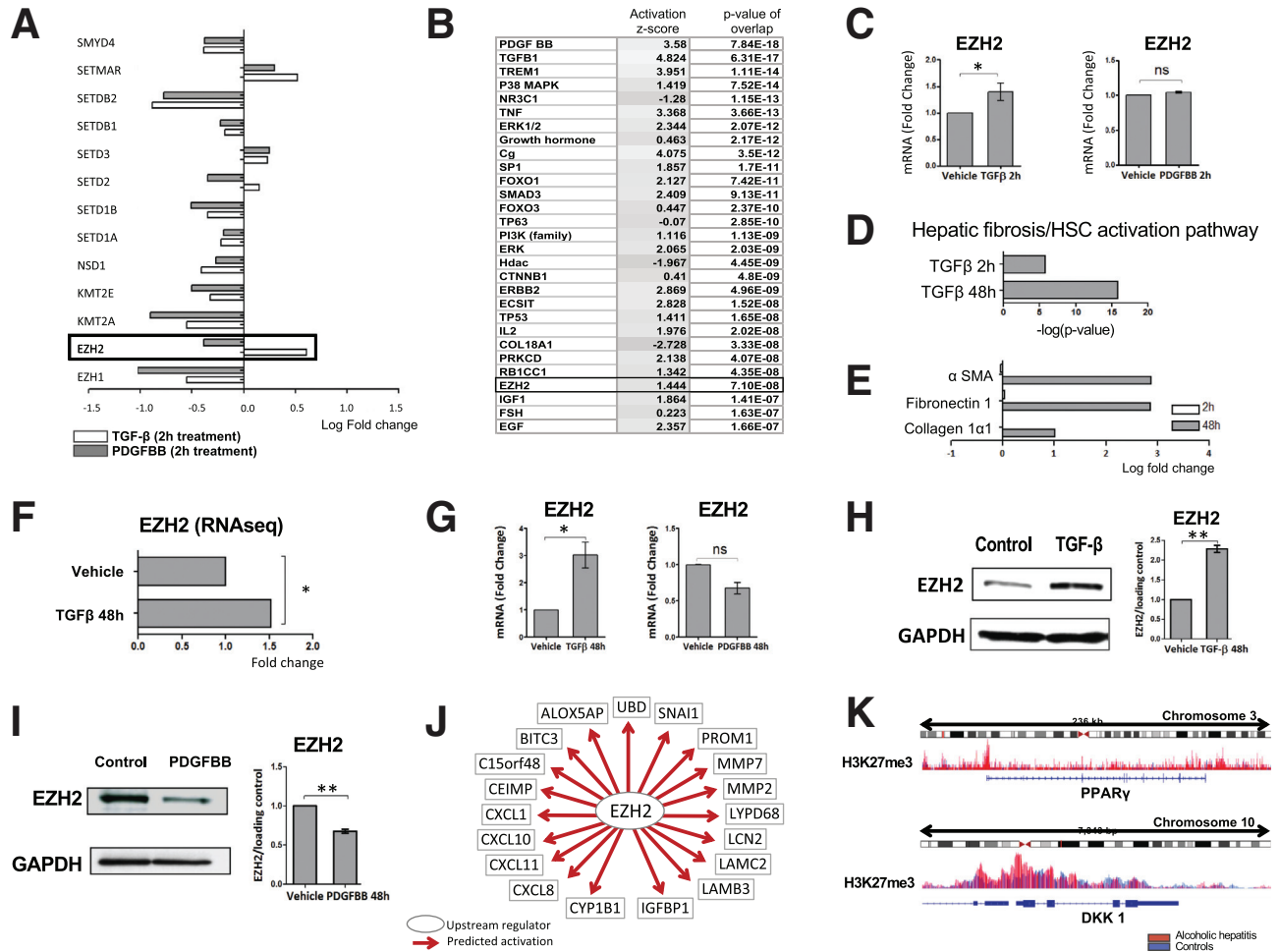


Figure 2. EZH2 is up-regulated in HSCs treated with TGF-β but not with PDGF-BB. (A) Differential expression analysis of HMTs in the RNA sequencing showed that EZH2 is up-regulated significantly after TGF-β but not PDGF-BB treatment (only HMTs with $P < .05$ and FDR < 0.05 are shown). (B) IPA identified EZH2 as an upstream regulator in HSCs treated with TGF-β (activation z-score, 1.444) (C) Quantitative PCR analysis confirmed that EZH2 is up-regulated after stimulation with TGF-β ($*P = .0286$), although there were no differences with PDGF-BB (NS: $P = .1$) at 2 hours. (D) RNA sequencing of HSCs treated with TGF-β for 48 hours confirmed an increasing profibrotic effect by means of higher activation of the hepatic fibrosis canonical pathway and (E) increased significant expression of profibrotic genes: α-SMA (logFC, 2.785; $P = 1.25E-161$), fibronectin 1 (logFC, 2.860; $P = 5.95E-111$), and collagen 1α1 (logFC, 1.002; $P = 2,04E-19$). (F) RNA sequencing of HSCs treated with TGF-β for 48 hours confirmed the consistent up-regulation of EZH2 ($*P = 4.50E-14$ and FDR = 3,76E-13). (G) RNA sequencing results were confirmed by quantitative PCR (NS: $P > .05$; $*P < .05$). (H and I) Western blots and quantification graphs were consistent with previous results showing higher EZH2 expression after treatment with TGF-β ($**P = .0048$) vs PDGF-BB ($**P = .006$) at 48 hours. (J) RNA sequencing analysis performed in human liver samples with alcoholic hepatitis ($n = 7$) and controls ($n = 5$). IPA identified EZH2 as an important upstream regulator in alcoholic patients (activation z-score, 2.453; P value of overlap = 3.92E-10). Up-regulated genes consistent with activation of EZH2 are shown. (K) ChIP sequencing analysis confirmed a gain in H3K27me3 at the promoter of peroxisome proliferator-activated receptor γ (PPARγ) (top panel) and DKK1 (bottom panel) in this cohort (shown in red) as compared with controls (blue). The y-axis represents peak values of the histogram, and the x-axis shows the chromosomal location of the gene. Results from 3 independent experiments each performed in triplicate are shown. Paired t test. Data are expressed as means \pm SEM. GAPDH, glyceraldehyde-3-phosphate dehydrogenase.

To further show the effect of EZH2 inhibition in HSCs, we knocked down the gene using siRNA. Primary human HSCs were incubated with SignalSilence EZH2 siRNA I (Cell Signaling Technology, Danvers, MA) for 48 hours, and then treated with TGF-β or vehicle for another 48 hours. EZH2 knockdown was confirmed at the protein level (Figure 3E)

and, consistent with our previous results, down-regulation of EZH2 with the siRNA significantly attenuated the TGF-β-induced increase in fibronectin, α-SMA, and collagen 1α1 (Figure 3F). These results suggest that EZH2 inhibition contributes to attenuate TGF-β-dependent HSC activation and production of ECM proteins.

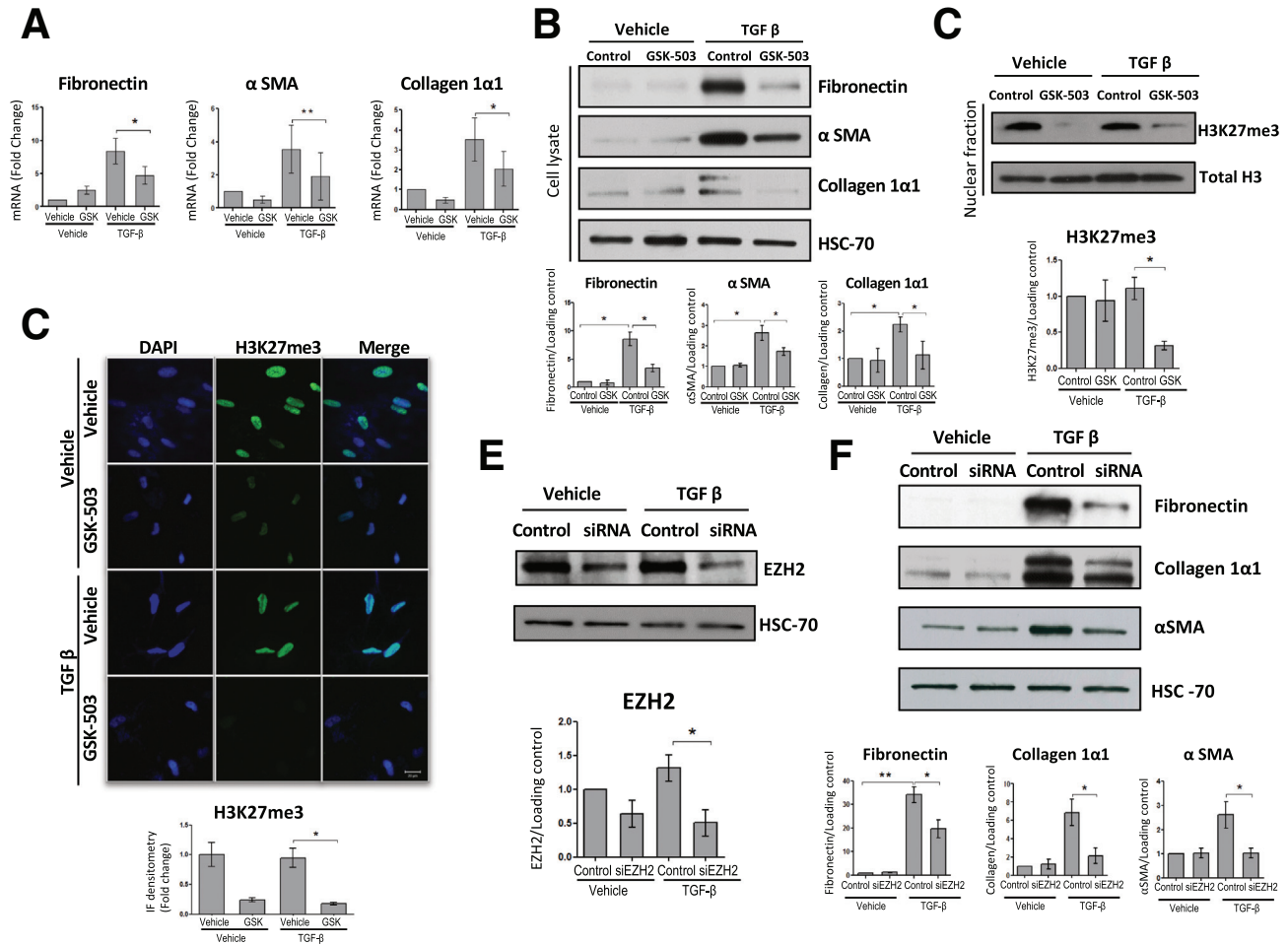


Figure 3. EZH2 inhibition attenuates HSC activation. Primary human HSCs were treated for 48h with GSK-503 and TGF- β (A) mRNA levels of fibronectin ($P = .0407$), α SMA ($P = .0017$) and collagen 1 α 1 ($P = .0232$) were significantly decreased after treatment with GSK-503 in those cells activated with TGF- β . (B) Western blots and quantification graphs of fibronectin (vehicle vs vehicle-TGF- β ; $P = .0252$; vehicle-TGF- β vs GSK-503-TGF- β ; $P = .0206$), α SMA (vehicle vs vehicle-TGF- β ; $P = .0466$; vehicle-TGF- β vs GSK-503-TGF- β ; $P = .0452$), and collagen 1 α 1 (vehicle vs vehicle-TGF- β ; $P = .0450$; vehicle-TGF- β vs GSK-503-TGF- β ; $P = .0449$) showing the same effect at the protein level. (C) H3K27me3 significantly decreased in HSCs treated with TGF- β and GSK-503 ($P = .0486$). (D) The effect of the drug in H3K27me3 was also demonstrated by immunofluorescence ($P = .0268$). (E) EZH2 expression was effectively reduced with EZH2 siRNA ($P = .0494$). (F) Western blots and quantification graphs showed a decrease in fibronectin (control-vehicle vs control-TGF- β ; $P = .0095$; control-TGF- β vs siRNA-TGF- β ; $P = .0484$), α SMA ($P = .0455$) and collagen 1 α 1 ($P = .0171$) with the EZH2 siRNA. Paired t -test. Data are expressed as means \pm SEM. All P values represent at least 3 different experiments performed in triplicate. * $P < .05$; ** $P < .01$. DAPI, 4',6'-diamidino-2-phenylindole.

EZH2 Overexpression Promotes Production of ECM Proteins In Vitro

We next took an overexpression strategy to further investigate the effects of EZH2 in HSCs. We infected primary human HSCs with a plasmid encoding an overexpression mutant of EZH2 after 6 hours of serum starvation. As an experimental control, cells also were infected with an empty vector. After 48 hours, basal media was replaced and cells were treated with TGF- β for 48 hours. First, we confirmed the significant up-regulation of EZH2 at the mRNA level (Figure 4A), which led to a subsequent increase in fibronectin, α -SMA, and collagen 1 α 1 mRNA (Figure 4B). Finally, we confirmed that EZH2 adenoviral overexpression and the subsequent increase in H3K27me3 leads to a significant

increase in fibronectin protein expression as well (Figure 4C and D).

EZH2 Inhibition Attenuates Liver Fibrosis in Mice Treated With CCL₄ and BDL

Next, we assessed the effect of EZH2 inhibition in vivo. Wild-type (WT) mice were treated with olive oil or CCL₄ and GSK-503 or vehicle for 4 weeks. GSK-503 was administered intraperitoneally (IP) 3 times a week (1.5 mg/mouse). Administration of GSK-503 to mice attenuated CCL₄-induced fibrosis as assessed by Masson's Trichrome and Sirius red stains from paraffin-fixed liver tissues (Figure 5A). At the protein level, we found a significant up-regulation of EZH2

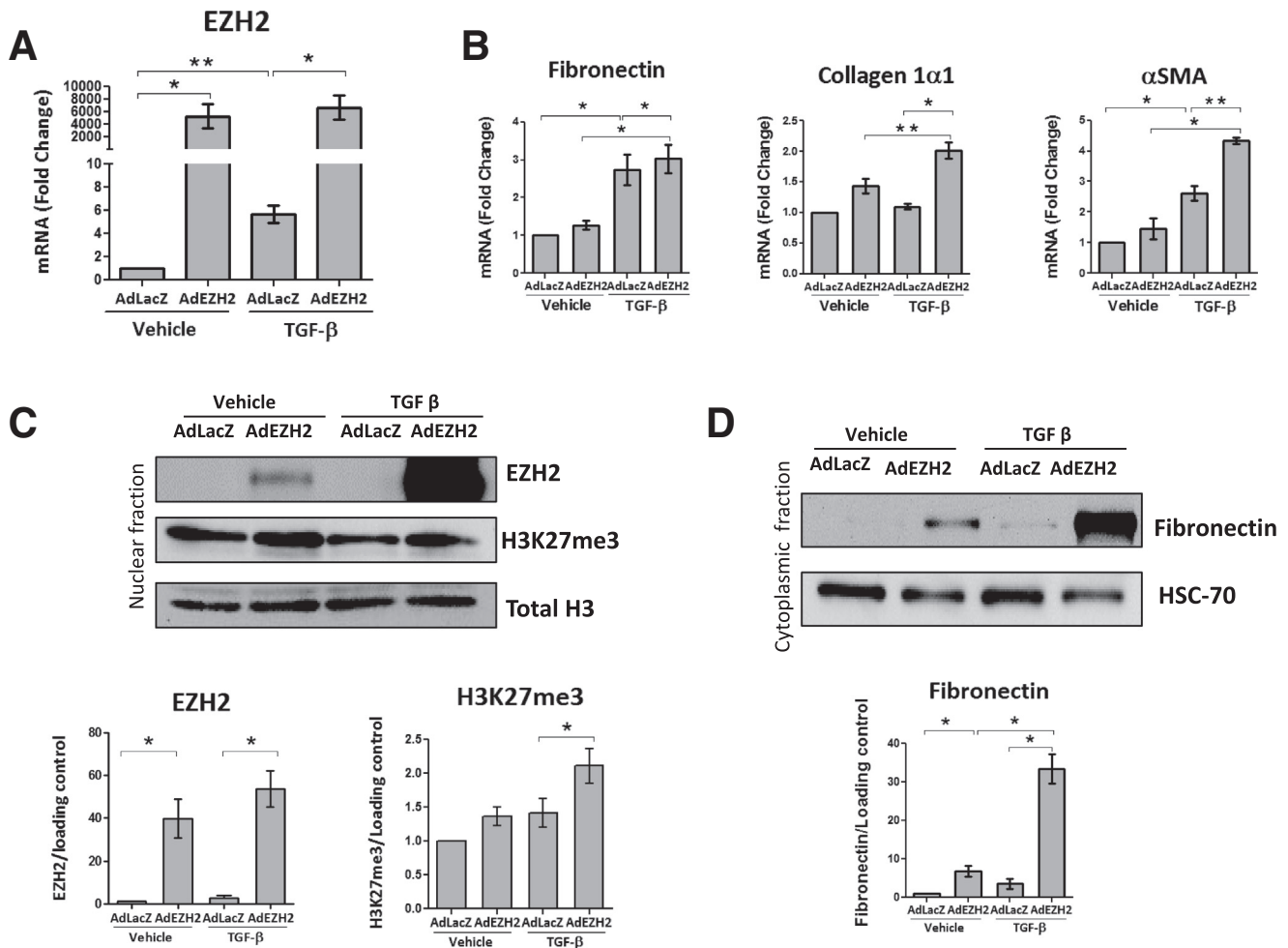


Figure 4. EZH2 adenoviral overexpression promotes ECM protein production. Primary human HSCs were infected with an adenovirus overexpressing EZH2 for 48 hours and then treated with TGF- β for another 48 hours. (A) Quantitative PCR confirmed the overexpression of EZH2 with the adenovirus (vehicle-AdLacZ vs vehicle-AdEZH2, $P = .0294$; vehicle-LacZ vs TGF- β -AdLacZ, $P = .0072$; and TGF- β -AdLacZ vs TGF- β -AdEZH2, $P = .0406$). (B) EZH2 overexpression significantly increased mRNA levels of fibronectin (vehicle-AdLacZ vs TGF- β -AdLacZ, $P = .0494$; vehicle-AdEZH2 vs TGF- β -AdEZH2, $P = .0221$; and TGF- β -AdLacZ vs TGF- β -AdEZH2, $P = .0315$), collagen 1 α 1 (vehicle-AdEZH2 vs TGF- β -AdEZH2, $P = .0040$; and TGF- β -AdLacZ vs TGF- β -AdEZH2, $P = .0127$), and α -SMA (vehicle-AdLacZ vs TGF- β -AdLacZ, $P = .0188$; vehicle-AdEZH2 vs TGF- β -AdEZH2, $P = .0228$; and TGF- β -AdLacZ vs TGF- β -AdEZH2, $P = .0067$). (C) EZH2 overexpression was confirmed at the protein level (vehicle-AdLacZ vs vehicle-AdEZH2, $P = .0496$; and TGF- β -AdLacZ vs TGF- β -AdEZH2, $P = .0316$) and paralleled the increase of H3K27me3 in cells treated with TGF- β ($P = .0478$) (upper panel: Western blot; lower panel: quantification graph). (D) Fibronectin protein expression increased as a result of the EZH2 adenovirus infection as shown by Western blot (upper panel) and the quantification graph (lower panel) (vehicle-AdLacZ vs vehicle-AdEZH2, $P = .0493$; vehicle-AdEZH2 vs TGF- β -AdEZH2, $P = .0186$; TGF- β -AdLacZ vs TGF- β -AdEZH2, $P = .0264$). Paired t test. Data are expressed as means \pm SEM. All P values represent at least 3 different experiments performed in triplicate. * $P < .05$; ** $P < .01$.

in all mice treated with CCL₄ compared with those who received olive oil (Figure 5B). However, the H3K27me3 mark was attenuated significantly in response to GSK-503 administration as assessed by Western blot (Figure 5B). Collagen 1 α 1 and α -SMA protein expression paralleled the H3K27me3 reduction (Figure 5B). Hydroxyproline measurement from tissue lysates also showed a reduction in collagen deposition in CCL₄ plus GSK-503 administered mice as compared with mice receiving CCL₄ alone (Figure 5C).

To corroborate the in vivo effect of EZH2 inhibition in an alternative model of liver fibrosis, we performed BDL in WT mice. Seven days after surgery, GSK-503 was administered IP every 48 hours (1.5 mg/mouse) and, finally, mice were killed 15 days after the intervention. Similar to the experiment with CCL₄, mice subjected to BDL but treated with GSK-503 showed decreased collagen and α -SMA protein expression (Figure 5D). Sirius red and Masson's Trichrome stains also showed decreased ductal proliferation

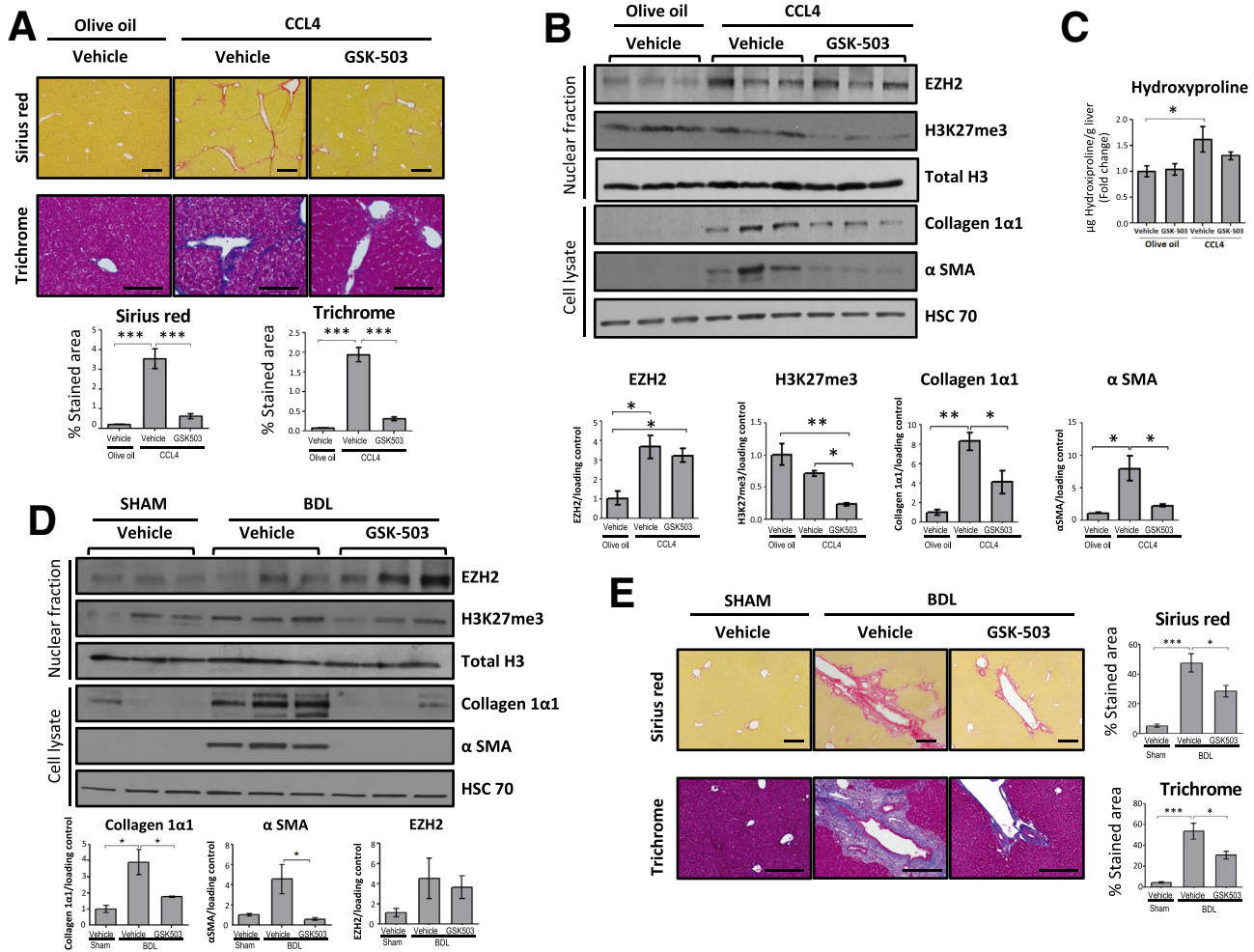


Figure 5. EZH2 inhibition attenuates liver fibrosis in vivo. C57/BL6 mice were treated with olive oil and either GSK-503 ($n = 6$) or vehicle ($n = 6$), and CCL₄ and either GSK-503 ($n = 6$) or vehicle ($n = 6$) for 4 weeks. (A) Paraffin liver sections of mice treated with CCL₄ or olive oil and GSK-503 or vehicle. CCL₄-induced liver injury was attenuated by GSK-503 in Sirius red (5x) and Masson's Trichrome (20x) stain. (B) Western blots and quantification graphs from mice treated with CCL₄ and GSK-503 showed a significant decrease in H3K27me3 and, subsequently, a significant decrease in collagen 1 α 1 and α -SMA. EZH2 increased significantly in mice treated with CCL₄. (C) Collagen deposition measured by hydroxyproline assay was consistent with previous results. (D) C57/BL6 mice were subjected to BDL and treated with GSK-503 ($n = 5$) or vehicle ($n = 6$), or underwent sham intervention and received GSK-503 ($n = 6$) or vehicle ($n = 6$). Mice that were treated with GSK-503 showed a significant decrease in collagen 1 α 1 and α -SMA. EZH2 showed a nonsignificant increase in BDL group vs sham. (E) Paraffin-embedded liver sections were stained with Sirius red (5x) and Masson's Trichrome (10x). Data are expressed as means \pm SEM. All statistical calculations were performed with analysis of variance and the Bonferroni comparison post-test. *** $P < .0001$; ** $P < .005$; * $P < .05$.

(Figure 5E). These in vivo results indicate that EZH2 inhibition attenuates murine liver fibrosis.

Discussion

Delineation of redundant and distinct signaling downstream of canonical TGF- β and PDGF pathways is important for HSC biology and potential therapeutic interventions. In this study, we identify a new role of the HMT EZH2 in hepatic fibrosis through preferential induction by TGF- β as compared with PDGF-dependent pathways. We show that EZH2 inhibition attenuates HSC activation and fibrosis in vivo, and, conversely, EZH2 overexpression promotes

ECM protein deposition. This is of particular interest given the number of EZH2 pharmacologic inhibitors that are under drug development and clinical evaluation, particularly in the neoplasia space.¹⁷⁻²⁰

TGF- β and PDGF are critically involved in HSC transdifferentiation. TGF- β is canonically the more notable profibrotic stimulus,⁴ whereas PDGF is more prominent for its mitogenic and motogenic effects on HSCs.⁵ The comparison analysis between HSCs treated either with TGF- β or PDGF showed a predominantly profibrotic role of TGF- β in HSC activation along with overlapping regulation of multiple genes with PDGF. Interestingly, the analysis also showed that this effect may be related to the

fact that TGF- β stimulation also activates other growth factors involved in HSC activation, including PDGFA and B, CTGF, VEGFA, and fibroblast growth factor 2. Therefore, TGF- β plays a key role in HSC activation, and epigenetic modifications may contribute to this process. Some studies have explored the epigenetic regulation of TGF- β signaling in other biological contexts; it has been shown that DNA methylation,^{21,22} microRNAs,²³ and histone modifications²⁴ regulate gene expression of key effectors of the pathway; however, evidence in liver fibrosis is scarcer.²⁵ Therefore, the specific contribution of epigenetics on TGF- β -induced HSC activation was the focus of our current investigation.

There is a growing interest in epigenetic drug development for investigational and therapeutic purposes.^{26,27} Given the emergence of the oncogene EZH2 from our RNA sequencing data set, we focused on the role of this HMT in TGF- β -induced HSC activation and liver fibrosis in vivo. Some prior studies also have addressed histone modifications and liver fibrosis including EZH2. For example, it has been reported that the histone methyltransferase inhibitor, 3-deazaneplanocin A, may halt the progression of liver fibrosis in mice treated with CCL₄.²⁸ However, 3-deazaneplanocin, although initially considered a selective EZH2 inhibitor, showed poor specificity because it altered multiple histone methylation marks. Here, we show the specific role of EZH2 by means of a targeted knockdown with a siRNA. Mann et al¹¹ also uncovered an interesting link between methyl CpG binding protein 2, miR132, and EZH2. They showed that EZH2 may contribute to peroxisome proliferator-activated receptor γ transcriptional silencing in a relay pathway along with methyl CpG binding protein 2 and microRNA132. It also has been reported that EZH2-mediated repression of Dkk-1 may promote activation of the Wnt/ β -catenin pathway,²⁹ which has been shown to contribute to HSC transdifferentiation.³⁰ Our results consistently confirm the profibrotic role of EZH2 in vitro and in vivo, corroborating its potential as a target for anti-fibrotic therapy.

Several possible mechanisms may explain the profibrotic effect of EZH2. In addition to the previously mentioned role as a repressor of important negative regulators of liver fibrosis,^{11,29} Xiao et al¹² showed that inhibition of EZH2 also may reduce TGF- β -induced differentiation of human lung fibroblasts into myofibroblasts, preventing Smad2/3 nuclear translocation. On the other hand, it also has been shown that EZH2 mediates the development of renal fibrosis by down-regulating the expression of Smad7, a negative regulator of the TGF- β signaling pathway.¹³ Finally, in the liver, EZH2 also contributes to other processes implicated in fibrogenesis such as proliferation and epithelial-to-mesenchymal transition.^{31,32} Therefore, it is conceivable that EZH2 promotes liver fibrosis by targeting different pathways, and in coordination with other epigenetic marks. Because of the predominant nuclear localization of EZH2, and the small percentage of HSCs in liver tissues, specific EZH2 staining of activated HSCs in human samples has been difficult, however, increased global expression of EZH2 has been shown in mice treated with CCL₄ vs controls,²⁴ and in

patients with liver failure and liver cancer as compared with healthy controls.^{33,34}

EZH2 is well known for its role in H3K27me₃, leading to chromatin compaction and gene silencing. However, chromatin-independent functions also have been shown. EZH2 may drive methylation of nonhistone proteins such as transcription factors involved in cell adhesion and migration,³⁵ actin polymerization,³⁶ or T-cell development,³⁷ among others.^{38,39} It is conceivable that these noncanonical roles of EZH2 also could contribute to the effects we observed.

Finally, multiple evidences have shown that EZH2 is highly expressed and plays a key role in several types of cancer.^{9,40–42} It has been identified as one of the most deregulated epigenetic modulators in hepatocellular carcinoma (HCC),^{10,43} promoting hepatocarcinogenesis through different mechanisms. Specifically, EZH2 contributes to liver cancer through modulation of different tumor-suppressor microRNAs,^{44,45} long noncoding RNAs,⁴⁶ or regulating the cell cycle,⁴⁷ among other processes. It also has been shown that EZH2 gene expression levels in HCC specimens may have prognostic implications.^{34,47,48} Recently, some evidence has suggested that EZH2 inhibition contributes to HCC immune-mediated eradication by natural killer cells.⁴⁹ Thus, EZH2 could represent a potential link between fibrosis and the ensuing HCC that frequently occurs in the fibrotic liver.

In summary, in this study, we present evidence that supports the role for the HMT EZH2 in promoting TGF- β -but not PDGF-dependent fibrogenic pathways. In addition, we show that EZH2 inhibition attenuates HSC activation in vitro and liver fibrosis in vivo. Consequently, EZH2 modulation may be a promising epigenetic target for liver fibrosis.

Materials and Methods

Cell culture. Primary human HSCs (5300; ScienCell Research Laboratories, Carlsbad, CA) were grown in Dulbecco's modified Eagle medium (11965092; Life Technologies, Carlsbad, CA) containing 10% fetal bovine serum (FBS) (F4135; Sigma-Aldrich, St. Louis, MO) and 1% penicillin/streptomycin (15140122; Life Technologies). Cells were treated with GSK-503 (ApexBio, Houston, TX) (10 mmol/L) and/or TGF- β (240-B; R&D Systems, Minneapolis, MN) (10 ng/mL) and/or PDGF-BB (P3201; Sigma-Aldrich) (10 ng/mL) for 48 hours. All cell lines were maintained under standard tissue culture conditions (37°C, 5% CO₂ incubator).

RNA sequencing. RNA sequencing and bioinformatics analyses were conducted in collaboration with the Mayo Medical Genomics Facility. The quality of the RNA was assessed by the Mayo Gene Expression Core using Agilent Bioanalyzers. RNA sequencing was performed as paired-end base reads on an Illumina HiSeq 2000 with 3 samples per lane, using the TruSeq SBS Sequencing Kit, version 3. Base calling was performed using Illumina's (San Diego, CA) RTA version 1.12.4.2. Bioinformatics were performed with the assistance of the Mayo Division of Biostatistics and

Table 2. Mice and Human Primer Sequences

h EZH2	Forward 5'-CCCTGACCTCTGTCTTACTTGTGGA-3' Reverse 3'-ACGTCAGATGGTGCCAGAAATA-3'
h Fibronectin	Forward 5'-GATAAATCAACAGTGGGAGC-3' Reverse 5'-CCCAGATCATGGAGTCTTTA-3'
h α -SMA	Forward 5'-GACAGCTACGTGGGTGACGAA-3' Reverse 5'-TTTTCCATGTCGTCCAGTTG-3'
h Collagen 1 α 1	Forward 5'-CCCAGGTTTCAGAGACAACCTC-3' Reverse 5'-TCCACATGCTTTATCCAGACATC-3'
h GAPDH	Forward 5'-CCAGGCTGCTTTAACTCT-3' Reverse 5'-GGACTCCACGACGACTCA-3'
m β -actin	Forward 5'-AGAGGGAAATCGTGCGTGAC-3' Reverse 5'-CAATAGTGATGACCTGGCCGT-3'
m Collagen 1 α 1	Forward 5'-GAGCGGAGAGTACTGGATCG-3' Reverse 5'-GCTTCTTTTCCCTTGGGGTTC-3'
m EZH2	Forward 5'-TCCCGTTAAAGACCCTGAATG-3' Reverse 5'-TGAAAGTGCCATCCTGATCC-3'
m Fibronectin	Forward 5'-GTGGCTGCCTTCAACTTCTC-3' Reverse 5'-GTGGGTTGCAAACCTTCAAT-3'
m α -SMA	Forward 5'-AAACAGGAATACGACGAAG-3' Reverse 5'-CAGGAATGATTTGAAAGGA-3'
m EZH2	Forward 5'-TCCCGTTAAAGACCCTGAATG-3' Reverse 5'-TGAAAGTGCCATCCTGATCC-3'

GAPDH, glyceraldehyde-3-phosphate dehydrogenase; h, human; m, mouse.

Informatics. Analysis of each sample (alignment statistics, in-depth quality-control metrics, and gene and exon expression levels) was performed using Mayo Clinic's MAPRSeq (Rochester, MN) v1.2. Reads were mapped using Tophat (Baltimore, MD) version 2.0.6 against the hg19 reference genome, and gene counts were produced using high-throughput sequencing. Differential expression analyses between samples were computed using an edgeR version 3.3.8 algorithm. A whole-genome heat map was created with the Heatmapper web server as described elsewhere.⁵⁰

ChIP sequencing. Liver tissue was collected from patients with alcoholic hepatitis undergoing early liver transplantation (n = 7), and from nondiseased livers (n = 5).¹⁴ ChIP sequencing was performed for H3K27me3 and data were processed using Mayo Clinic bioinformatics pipelines. Regions showing differential occupancy by individual histone marks were identified and assigned to promoters.

Quantitative reverse-transcription polymerase chain reaction. The RNeasy kit (Qiagen) was used to extract total RNA from cells (and mouse tissue) according to the manufacturer's instructions. RNA was reverse-transcribed using the SuperScript III System (Invitrogen, Carlsbad, CA), and TaqMan-based real-time reverse-transcription polymerase chain reaction (PCR) was performed according to the manufacturer's instructions (Applied Biosystems, Foster City, CA). Amplification of glyceraldehyde-3-phosphate dehydrogenase (or β -actin) was performed in the same reaction for the respective samples as an internal control. Each experiment was performed at least in triplicate. Real-time PCR conditions were as follows: 95°C for 5 minutes, then 40 cycles of 95°C for 15 seconds, 60°C for

Table 3. Antibodies Used in Western Blot Analysis

Primary antibody	Company and product number
EZH2	Cell Signaling 5246
H3K27me3	Abcam Ab6147
GAPDH	Invitrogen AM4300
Fibronectin	Santa Cruz sc-9068
HSC 70	Santa Cruz sc-7298
Collagen 1	Southern Biotech (Birmingham, AL) 1310-01
α -SMA	Abcam ab5694
Histone 3	Abcam ab1791

GAPDH, glyceraldehyde-3-phosphate dehydrogenase.

30 seconds, 72°C for 30 seconds, and a final extension at 72°C for 30 seconds. Mice and human primer sequences are listed in Table 2.

Western blot analysis. HSCs or liver tissues were lysed and prepared for Western blot analysis as described previously.⁵¹ Immunoblot analysis was performed according to the protocol recommended for individual antibodies as listed in Table 3. Immunoreactive bands were visualized using horseradish-peroxidase-conjugated secondary antibody and an enhanced chemiluminescent system (sc-2048, Immuno Cruz; Santa Cruz Biotechnology, Inc, Dallas, TX; or WBLUR0100, Luminata Crescendo, Millipore Sigma, Burlington, MA). For some experiments, the protein nuclear fraction was isolated and lysates then were sonicated for 15 seconds (amplitude, 5%).

Cell immunofluorescence. HSCs were plated at 80% confluence on 8-well chamber slides (177402; Lab-Tek, Sigma-Aldrich) precoated with collagen (C4243; Sigma-Aldrich). After 24 hours of culture, cells were washed with 1 \times phosphate-buffered saline and incubated with GSK-503 (ApexBio) (10 mmol/L) and/or TGF- β (240-B; R&D Systems) (10 ng/mL) for 48 hours. Cells then were fixed in 4% paraformaldehyde and nonspecific sites were blocked with 10% FBS. Cells then were incubated overnight at 4°C in primary antibody to detect H3K27me3 (1:200) (ab6147; Abcam, Cambridge, United Kingdom) diluted in 1% bovine serum albumin. After washing, cells were incubated in fluorochrome-coupled secondary antibody diluted in 1 \times phosphate-buffered saline for 1 hour at room temperature. All secondary antibodies were provided by Life Technologies and used at 1:200.

RNA interference knockdown. After overnight starvation, human HSCs were transfected with 100 nmol/L of siRNA (SignalSilence Ezh2 siRNA I 6509; Cell Signaling Technology) using Oligofectamine (12252011; Invitrogen) according to the manufacturer's instructions. Forty-eight hours later, media was replaced and TGF- β (240-B; R&D Systems) (10 ng/mL) was added for 48 hours.

Adenoviral transfection. Epitope-tagged (6XHis-Xpress) EZH2 α was generated as recombinant adenovirus by the Gene Transfer Vector Core at the University of Iowa. Empty

vector (pacAD5 CMV) was used as the experimental control as described elsewhere.⁵² Primary human HSCs were infected with the adenovirus (8^{10} pfu/mL) after a 6-hour starvation. Forty-eight hours later, 1% FBS Dulbecco's modified Eagle medium was replaced and cells were treated with TGF- β (240-B; R&D Systems) (10 ng/mL) for another 48 hours.

Liver Fibrosis In Vivo Models

CCL₄ and GSK-503 treatment. WT C57/BL6 mice (age, 8 wk) were purchased from Envigo (Huntingdon, United Kingdom). We chose female mice because to their higher susceptibility to liver injury.⁵³ CCL₄ was injected IP twice a week at 4 μ L/g/body (CCL₄/olive oil, 1:3) for 4 weeks. GSK-503 also was administered IP 3 times a week (1.5 mg/mouse) alternating with CCL₄ on different days. Twenty-four hours after the final injection, mice were killed and livers were harvested. Fibrosis was analyzed by Sirius Red and Masson's Trichrome stains (paraffin-embedded tissues), hydroxyproline analysis, quantitative PCR, immunoblotting, and immunofluorescence. All animal experiments followed protocols approved by the Mayo Clinic Institutional Animal Care and Use Committee.

BDL model. BDL was performed as previously described⁵⁴ in WT 8-week-old female mice. Seven days after the surgery, the animals were injected IP with GSK-503 (1.5 mg/mouse) every 48 hours and killed 15 days later.

Hydroxyproline assay. Hepatic hydroxyproline levels were quantified using a colorimetric assay. Frozen liver tissues (50–100 mg) were hydrolyzed in 6 N hydrochloric acid at 100°C for 18 hours. Samples then were dried using a speed vacuum overnight. The precipitates were suspended in distilled water and transferred to 0.22- μ m-filter centrifuge tubes. In duplicates, 5 μ L of the filtered samples were incubated with 50 μ L of chloramine-T and distilled water for 20 minutes. Then, 50 μ L of Ehrlich-perchloric acid was added and incubated for 15 minutes at 65°C and 20 minutes at room temperature. The absorbance was read at 561 nm using a spectrophotometer, and the results were normalized by the weight of each sample.

Statistical Analysis

Results are expressed as the means of 3 or more independent experiments. Analysis of variance with Bonferroni post-test, nonparametric 2-tailed *t* test (Mann-Whitney), or paired *t* test for cell culture experiments were used to assess the statistical significance between groups as appropriate with GraphPad Prism 5 software (GraphPad Software, Inc, La Jolla, CA). A *P* value less than .05 was considered statistically significant.

All authors had access to the study data and reviewed and approved the final manuscript.

References

- Hernandez-Gea V, Friedman SL. Pathogenesis of liver fibrosis. *Annu Rev Pathol* 2011;6:425–456.
- Perepelyuk M, Terajima M, Wang AY, Georges PC, Janmey PA, Yamauchi M, Wells RG. Hepatic stellate cells and portal fibroblasts are the major cellular sources of collagens and lysyl oxidases in normal liver and early after injury. *Am J Physiol Liver Physiol* 2013; 304:G605–G614.
- Tsuchida T, Friedman SL. Mechanisms of hepatic stellate cell activation. *Nat Rev Gastroenterol Hepatol* 2017; 14:397–411.
- Friedman SL. Hepatic stellate cells: protean, multifunctional and enigmatic cells of the liver. *Physiol Rev* 2008; 88:125–172.
- Kikuchi A, Pradhan-Sundd T, Singh S, Nagarajan S, Loizos N, Monga SP. Platelet-derived growth factor receptor α contributes to human hepatic stellate cell proliferation and migration. *Am J Pathol* 2017; 187:2273–2287.
- Berger SL, Kouzarides T, Shiekhattar R, Shilatifard A. An operational definition of epigenetics. *Genes Dev* 2009; 23:781–783.
- Moran-Salvador E, Mann J. Epigenetics and liver fibrosis. *Cell Mol Gastroenterol Hepatol* 2017;4:125–134.
- Cao R, Wang L, Wang H, Xia L, Erdjument-Bromage H, Tempst P, Jones RS, Zhang Y. Role of histone H3 lysine 27 methylation in polycomb-group silencing. *Science* 2002;298:1039–1043.
- Yamagishi M, Uchamaru K. Targeting EZH2 in cancer therapy. *Curr Opin Oncol* 2017;29:375–381.
- Au SL, Wong CC, Lee JM, Fan DN, Tsang FH, Ng IO, Wong CM. Enhancer of zeste homolog 2 epigenetically silences multiple tumor suppressor microRNAs to promote liver cancer metastasis. *Hepatology* 2012; 56:622–631.
- Mann J, Chu DC, Maxwell A, Oakley F, Zhu NL, Tsukamoto H, Man DA. MeCP2 controls an epigenetic pathway that promotes myofibroblast transdifferentiation and fibrosis. *Gastroenterology* 2010;138:705–714.
- Xiao X, Senavirathna LK, Gou X, Huang C, Liang Y, Liu L. EZH2 enhances the differentiation of fibroblasts into myofibroblasts in idiopathic pulmonary fibrosis. *Physiol Rep* 2016;4:e12915.
- Zhou X, Zang X, Ponnusamy M, Masucci MV, Tolbert E, Gong R, Zhao TC, Liu N, Bayliss G, Dworkin LD, Zhuang S. Enhancer of zeste homolog 2 inhibition attenuates renal fibrosis by maintaining Smad7 and phosphatase and tensin homolog expression. *J Am Soc Nephrol* 2016;27:2092–2108.
- Arab JP, Cao S, Lee JH, Argemi J, Massey V, Ordog T, Mathurin P, Yan H, Bataller R, Shah V. Transcriptional dysregulation of inflammatory gene networks in alcoholic hepatitis is associated with genomewide reconfiguration of epigenetic states. *Gastroenterology* 2018; 154:s1109.
- Béguelin W, Popovic R, Teater M, Jiang Y, Bunting KL, Rosen M, Shen H, Yang SN, Wang L, Ezponda T, Martinez-Garcia E, Zhang H, Zheng Y, Verma SK, McCabe MT, Ott HM, Van Aller GS, Kruger RG, Liu Y, McHugh CF, Scott DW, Chung YR, Kelleher N, Shaknovich R, Creasy CL, Gascoyne RD, Wong KK, Cerchietti L, Levine RL, Abdel-Wahab O, Licht JD,

- Elemento O, Melnick AM. EZH2 is required for germinal center formation and somatic EZH2 mutations promote lymphoid transformation. *Cancer Cell* 2013; 23:677–692.
16. Zingg D, Debbache J, Schaefer SM, Tuncer E, Frommel SC, Cheng P, Arenas-Ramirez N, Haeusel J, Zhang Y, Bonalli M, McCabe MT, Creasy CL, Levesque MP, Boyman O, Santoro R, Shakhova O, Dummer R, Sommer L. The epigenetic modifier EZH2 controls melanoma growth and metastasis through silencing of distinct tumour suppressors. *Nat Commun* 2015;6:6051.
 17. Italiano A, Soria JC, Toulmonde M, Michot JM, Lucchesi C, Varga A, Coindre JM, Blakemore SJ, Clawson A, Suttle B, McDonald AA, Woodruff M, Ribich S, Hedrick E, Keilhack H, Thomson B, Owa T, Copeland RA, Ho PTC, Ribrag V. Tazemetostat, an EZH2 inhibitor, in relapsed or refractory B-cell non-Hodgkin lymphoma and advanced solid tumours: a first-in-human, open-label, phase 1 study. *Lancet Oncol* 2018; 19:649–659.
 18. Hussein YR, Sood AK, Bandyopadhyay S, Albashiti B, Semaan A, Nahleh Z, Roh J, Han HD, Lopez-Berestein G, Ali-Fehmi R. Clinical and biological relevance of enhancer of zeste homolog 2 in triple-negative breast cancer. *Hum Pathol* 2012;43:1638–1644.
 19. Kurmasheva RT, Sammons M, Favours E, Wu J, Kurmashev D, Cosmopoulos K, Keilhack H, Klaus CR, Houghton PJ, Smith MA. Initial testing (stage 1) of tazemetostat (EPZ-6438), a novel EZH2 inhibitor, by the pediatric preclinical testing program. *Pediatr Blood Cancer* 2017;64:e26218.
 20. Agulnik M, Tannir NM, Pressey JG, Gounder MM, Cote GM, Roche M, Doleman S, Blakemore SJ, Clawson A, Daigle S, Tang J, Ho PTC, Demetri JD. A phase II, multicenter study of the EZH2 inhibitor tazemetostat in adult subjects with INI1-negative tumors or relapsed/refractory synovial sarcoma. *J Clin Oncol* 2016; 34:s15.
 21. Matsumura N, Huang Z, Mori S, Baba T, Fujii S, Konishi I, Iversen ES, Berchuck A, Murphy SK. Epigenetic suppression of the TGF-beta pathway revealed by transcriptome profiling in ovarian cancer. *Genome Res* 2011; 21:74–82.
 22. Watson CJ, Collier P, Tea I, Neary R, Watson JA, Robinson C, Phelan D, Ledwidge MT, McDonald KM, McCann A, Sharaf O, Baugh JA. Hypoxia-induced epigenetic modifications are associated with cardiac tissue fibrosis and the development of a myofibroblast-like phenotype. *Hum Mol Genet* 2014; 23:2176–2188.
 23. Li L, Shi JY, Zhu GQ, Shi B. MiR-17-92 cluster regulates cell proliferation and collagen synthesis by targeting TGFB pathway in mouse palatal mesenchymal cells. *J Cell Biochem* 2012;113:1235–1244.
 24. Gjaltema RAF, de Rond S, Rots MG, Bank RA. Pro-collagen lysyl hydroxylase 2 expression is regulated by an alternative downstream transforming growth factor β -1 activation mechanism. *J Biol Chem* 2015; 290:28465–28476.
 25. Fan Z, Hao C, Li M, Dai X, Qin H, Li J, Xu H, Wu X, Zhang L, Fang M, Zhou B, Tian W, Xu Y. MKL1 is an epigenetic modulator of TGF- β induced fibrogenesis. *Biochim Biophys Acta* 2015;1849:1219–1228.
 26. Hardy T, Mann DA. Epigenetics in liver disease: from biology to therapeutics. *Gut* 2016;65:1895–1905.
 27. Kronfol MM, Dozmorov MG, Huang R, Slattum PW, McClay JL. The role of epigenomics in personalized medicine. *Expert Rev Precis Med Drug Dev* 2017; 2:33–45.
 28. Zeybel M, Luli S, Sabater L, Hardy T, Oakley F, Leslie J, Page A, Moran Salvador E, Sharkey V, Tsukamoto H, Chu DCK, Singh US, Ponzoni M, Perri P, Di Paolo D, Mendivil EJ, Mann J, Mann DA. A proof-of-concept for epigenetic therapy of tissue fibrosis: inhibition of liver fibrosis progression by 3-deazaneplanocin A. *Mol Ther* 2017;25:218–231.
 29. Yang Y, Chen XX, Li WX, Wu XQ, Huang C, Xie J, Zhao YX, Meng XM, Li J. EZH2-mediated repression of Dkk1 promotes hepatic stellate cell activation and hepatic fibrosis. *J Cell Mol Med* 2017;21:2317–2328.
 30. Ge WS, Wang YJ, Wu JX, Fan JG, Chen YW, Zhu L. Beta-catenin is overexpressed in hepatic fibrosis and blockage of Wnt/beta-catenin signaling inhibits hepatic stellate cell activation. *Mol Med Rep* 2014;9:2145–2151.
 31. Zhao H, Wang Z, Tang F, Zhao Y, Feng D, Li Y, Hu Y, Wang C, Zhou J, Tian X, Yao J. Carnosol-mediated sir-tuin 1 activation inhibits enhancer of zeste homolog 2 to attenuate liver fibrosis. *Pharmacol Res* 2018; 128:327–337.
 32. Cho IJ, Kim YW, Han CY, Kim EH, Anderson RA, Lee CH, Hwang SJ, Kim SG. E-cadherin antagonizes transforming growth factor β 1 gene induction in hepatic stellate cells by inhibiting RhoA-dependent Smad3 phosphorylation. *Hepatology* 2010;52:2053–2064.
 33. Zhou T, Sun Y, Li M, Ding Y, Yin R, Li Z, Xie Q, Bao S, Cai W. Enhancer of zeste homolog 2-catalysed H3K27 trimethylation plays a key role in acute-on-chronic liver failure via TNF-mediated pathway. *Cell Death Dis* 2018; 9:590.
 34. Gao SB, Xu B, Ding LH, Zheng QL, Zhang L, Zheng QF, Li SH, Feng ZJ, Wei J, Yin ZY, Hua X, Jin GH. The functional and mechanistic relatedness of EZH2 and menin in hepatocellular carcinoma. *J Hepatol* 2014; 61:832–839.
 35. Gunawan M, Venkatesan N, Loh JT, Wong JF, Berger H, Neo WH, Li LY, La Win MK, Yau YH, Guo T, See PC, Yamazaki S, Chin KC, Gingras AR, Shochat SG, Ng LG, Sze SK, Ginhoux F, Su IH. The methyltransferase EZH2 controls cell adhesion and migration through direct methylation of the extranuclear regulatory protein talin. *Nat Immunol* 2015;16:505–516.
 36. Su IH, Dobenecker MW, Dickinson E, Oser M, Basavaraj A, Marqueron R, Viale A, Reinberg D, Wülfing C, Tarakhovskiy A. Polycomb group protein EZH2 controls actin polymerization and cell signaling. *Cell* 2005;121:425–436.
 37. Vasanthakumar A, Xu D, Lun AT, Kueh AJ, van Gisbergen KP, Iannarella N, Li X, Yu L, Wang D, Williams BR, Lee SC, Majewski IJ, Godfrey DI,

- Smyth GK, Alexander WS, Herold MJ, Kallies A, Nutt SL, Allan RS. A non-canonical function of EZH2 preserves immune homeostasis. *EMBO Rep* 2017;18:619–631.
38. Yan J, Li B, Lin B, Lee PT, Chung TH, Tan J, Selvarajan V, Ng SB, Yang H, Yu Q, Chng WJ. EZH2 phosphorylation by JAK3 mediates a switch to noncanonical function in natural killer/T-cell lymphoma. *Blood* 2016;128:948–958.
 39. Lawrence CL, Baldwin AS. Non-canonical EZH2 transcriptionally activates RelB in triple negative breast cancer. *PLoS One* 2016;11:e0165005.
 40. Yang YA, Yu J. EZH2, an epigenetic driver of prostate cancer. *Protein Cell* 2013;4:331–341.
 41. Yoo KH, Hennighausen L. EZH2 methyltransferase and H3K27 methylation in breast cancer. *Int J Biol Sci* 2011; 8:59–65.
 42. Wen Y, Cai J, Hou Y, Huang Z, Wang Z. Role of EZH2 in cancer stem cells: from biological insight to a therapeutic target. *Oncotarget* 2015;8:37974–37990.
 43. Chen Y, Lin MC, Wang H, Chan C, Jiang L, Ngai SM, Yu J, He ML, Shaw PC, Yew DT, Sung JJ, Kung HF. Proteomic analysis of EZH2 downstream target proteins in hepatocellular carcinoma. *Proteomics* 2007; 7:3097–3104.
 44. Chen S, Pu J, Bai J, Yin Y, Wu K, Wang J, Shuai X, Gao J, Tao K, Wang G, Li H. EZH2 promotes hepatocellular carcinoma progression through modulating miR-22/galectin-9 axis. *J Exp Clin Cancer Res* 2018;37:3.
 45. Cui S, Sun Y, Liu Y, Liu C, Wang J, Hao G, Sun Q. MicroRNA-137 has a suppressive role in liver cancer via targeting EZH2. *Mol Med Rep* 2017;16:9494–9502.
 46. Zhou M, Zhang XY, Yu X. Overexpression of the long non-coding RNA SPRY4-IT1 promotes tumor cell proliferation and invasion by activating EZH2 in hepatocellular carcinoma. *Biomed Pharmacother* 2017; 85:348–354.
 47. Feng H, Yu Z, Tian Y, Lee YY, Li MS, Go MYY, Cheung YS, Lai PB, Chan AM, To KF, Chan HL, Sung JJ, Cheng AS. A CCRK-EZH2 epigenetic circuitry drives hepatocarcinogenesis and associates with tumor recurrence and poor survival of patients. *J Hepatol* 2015;62:1100–1111.
 48. Sudo T, Utsunomiya T, Mimori K, Nagahara H, Ogawa K, Inoue H, Wakiyama S, Fujita H, Shirouzu K, Mori M. Clinicopathological significance of EZH2 mRNA expression in patients with hepatocellular carcinoma. *Br J Cancer* 2005;92:1754–1758.
 49. Bugide S, Green MR, Wajapeyee N. Inhibition of enhancer of zeste homolog 2 (EZH2) induces natural killer cell-mediated eradication of hepatocellular carcinoma cells. *Proc Natl Acad Sci U S A* 2018; 115:E3509–E3518.
 50. Babicki S, Arndt D, Marcu A, Liang Y, Grant JR, Maciejewski A, Wishard DS. Heatmapper: web-enabled heat mapping for all. *Nucleic Acids Res* 2016; 44:W147–W153.
 51. Maiers JL, Kostallari E, Mushref M, deAssuncao TM, Li Haiyang, Jalan-Sakrikar N, Huebert RC, Cao S, Malhi H, Shah VH. The unfolded protein response mediates fibrogenesis and collagen I secretion through regulating TANGO1 in mice. *Hepatology* 2017; 65:983–998.
 52. Grzenda A, Lomber G, Svingen P, Mathison A, Calvo E, Iovanna J, Xiong Y, Faubion W, Urrutia R. Functional characterization of EZH2 β reveals the increased complexity of EZH2 isoforms involved in the regulation of mammalian gene expression. *Epigenetics Chromatin* 2013;6:3.
 53. Mathews S, Xu M, Wang H, Bertola A, Gao B. Animals models of gastrointestinal and liver diseases. Animal models of alcohol-induced liver disease: pathophysiology, translational relevance, and challenges. *Am J Physiol Gastrointest Liver Physiol* 2014; 306:G819–G823.
 54. Tag CG, Sauer-Lehnen S, Weiskirchen S, Borkham-Kamphorst E, Tolba RH, Tacke F, Weiskirchen R. Bile duct ligation in mice: induction of inflammatory liver injury and fibrosis by obstructive cholestasis. *J Vis Exp* 2015;96.

Received April 23, 2018. Accepted September 7, 2018.

Correspondence

Address correspondence to: Vijay H. Shah, MD, Division of Gastroenterology and Hepatology, Mayo Clinic, 200 First Street SW, Rochester, Minnesota 55905. e-mail: shah.vijay@mayo.edu; fax: (507) 255-6318.

Acknowledgments

The authors thank Dr Enis Kostallari, Dr Guang Shi, Ms Theresa J. Johnson, and the Mayo Clinic Animal Core Facilities.

Author contributions

R. Martin-Mateos was responsible for the study concept and design, acquisition of data, analysis and interpretation of data, and drafting the manuscript; T. M. De Assuncao acquired data, analyzed and interpreted data, and provided material support; N. Jalan-Sakrikar acquired data, and analyzed and interpreted data; U. Yaqoob acquired data and provided material support; A. J. Mathison acquired data and provided material support; T. Greuter analyzed and interpreted data; S. Cao was responsible for the study concept and design, and analysis and interpretation of the data; J. P. Arab was responsible for the study concept and design, acquisition of data, and analysis and interpretation of the data; V. Verma acquired data, and analyzed and interpreted data; R. C. Huebert was responsible for the study concept and design, analysis and interpretation of the data, and critical revision of the manuscript for important intellectual content; G. Lomber was responsible for the study concept and design, and analysis and interpretation of data; P. Mathurin acquired data, and analyzed and interpreted the data; R. Urrutia was responsible for the study concept and design, analysis and interpretation of the data, and critical revision of the manuscript for important intellectual content; and Vijay H. Shah was responsible for the study concept and design, analysis and interpretation of the data, obtained funding, critical revision of the manuscript for important intellectual content, and study supervision.

Conflicts of interest

The authors disclose no conflicts.

Funding

Supported by National Institutes of Health R01 DK59615 and R01 AA21171 (V.H.S.), and the Spanish Association for the Study of the Liver (grant Juan Rodés 2016) (R.M.M.).